



Surface resonance properties of thin silver films with nanoparticles induced by pulsed-laser interference dewetting process

Hsuan-Kai Lin¹ · Ying-Chi Chen^{1,2} · Jia-Ren Lee² · Wei-Hua Lu¹ · Yuan-Jen Chang³

Received: 6 December 2021 / Accepted: 24 January 2022

© The Author(s), under exclusive licence to Springer-Verlag London Ltd., part of Springer Nature 2022

Abstract

Pure Ag thin films with a thickness of 10 nm were deposited on glass substrates using a thermal evaporator system. Nanoparticles were then induced in the films by a Michelson interferometer dewetting process. The particle size was found to decrease with an increasing laser power and exposure time. The minimum particle size was 150 nm for a laser power of 4 W and exposure time of 60 s. However, a smaller particle size of 110 nm was obtained by adopting a two-step exposure process with a rotation angle of 30° and an exposure time of 55 s. The absorption peak wavelength of the dewetted films increased with an increasing rotation angle. By contrast, a blue shift in the absorption spectrum occurred as the laser power increased. The half-height widths of the absorption peaks of the films dewetted using different rotation angles were wider than those of the films dewetted without rotation, indicating that the two-step rotation process resulted in a wider particle size distribution. Overall, the results show that the optical properties of the laser-dewetted Ag films are highly dependent on the interference parameters.

Keywords Michelson interferometer · Laser · Absorption spectra · Silver particle

1 Introduction

Periodic microstructures have many promising applications in the physics, chemistry, biology, optical, and sensing fields. Traditional methods for surface patterning and texturing involve photolithography and chemical processing. However, such methods are complex, time-consuming, and expensive, particularly for large-area applications. Thus, the feasibility for fabricating micro-gratings and other periodic structures using laser technology has attracted growing interest in recent decades [1–3]. Various laser-based methods for surface patterning have been proposed, including direct laser writing (DLW) [4], direct laser interference patterning (DLIP) [5], laser interference lithography (LIL) [6],

and laser-induced periodic surface structures (LIPSS) [7]. Ihlemann [8] used a simple UV laser ablation technique to pattern thin oxide films over a wide area through the structured superposition and cancellation of different waves. Several recent studies have demonstrated the feasibility for fabricating periodic structures on alloy surfaces using a two-beam interferometric technique based on femtosecond pulsed-laser radiation [9–11]. In the DLIP technique, two or more laser beams are overlapped in time and space, and the resulting interference pattern is used to create the desired grating microstructure on the irradiated surface. In such a technique, the geometry and size of the patterned microstructure can be controlled by adjusting the number of laser beams, beam polarization, and the interception angle between them [12, 13]. Compared to other laser patterning methods such as DLW and LIL, DLIP offers the possibility to create repetitive structures on the surface of many different materials, including stainless steel, aluminum alloy, titanium, and so on [11, 13, 14]. As a result, it is one of the most versatile and practical laser patterning techniques for industrial applications.

Metal nanoparticles (NPs) have many unique physical, electrical, and optical properties and have thus attracted significant attention in the literature [15, 16]. In the literature,

✉ Hsuan-Kai Lin
HKLin@mail.npust.edu.tw

¹ Graduate Institute of Materials Engineering, National Pingtung University of Science and Technology, Neipu, Taiwan

² Department of Physics, National Kaohsiung Normal University, Kaohsiung, Taiwan

³ Department of Mechanical Engineering, National Yunlin University of Science and Technology, Douliu, Taiwan

the rupture of the film or the irregularly shaped NPs transform into spherical NPs with smaller size dispersion. When thin films were irradiated by laser interference, particles can be produced in a short time [2, 17–19]. It is obvious that many studies have shown that NPs can be readily induced in thin film metallic systems through pulsed-laser-induced dewetting [2, 20]. Moreover, the particle size can be controlled by adjusting the power and duration of the laser pulses [21]. The local surface plasmon resonance (LSPR) wavelengths of Au [22], Ag [23], and Cu films with NPs fall in the visible region and are strongly enhanced in the presence of an electromagnetic field. As a result, metallic thin-film systems containing NPs have significant potential for a wide variety of sensing applications [24, 25]. Accordingly, the present study proposes a simple method for patterning periodic surface structures on thin Ag films using a Michelson interferometer system. The effects of the laser pulse power, exposure time, and optical path length difference of the Michelson interferometer on the NP size distribution are systematically examined for both a single-stage exposure process with a constant rotation angle and a two-step exposure process with a rotation angle ranging from 30 to 90°. The study then compares the absorption spectra of the Ag films processed using various laser pulse powers and rotation angles. It is shown that a blue shift in the absorption spectrum occurs as the laser power increases, whereas a red shift occurs as the rotation angle increases. Overall, the results show that the physical and optical properties of the interfered Ag thin films are both highly dependent on the interference parameters.

2 Experiment

Pure Ag thin films with a thickness of 10 nm were deposited on glass substrates using a thermal evaporator system (SSI-T500-1, Taiwan) with a base pressure of 6×10^{-6} torr and a maximum power of 2 kW. The surfaces of the thin films were then patterned using the Michelson interferometer system shown in Fig. 1 consisting of a pulsed-laser system (Fiber Laser; G3

SM Series, SPI, UK) with a wavelength of 1064 nm, a repetition rate of 100 kHz, and an irradiation power of 0.6–4 W. As shown in the left-hand schematic, the light emitted by the laser was incident on a beam splitter (R/T = 50/50, Newport) and separated into two paths. The reflected light was incident on mirror M_1 and was then passed back through the beam splitter and incident on the sample surface. The transmitted light was incident on mirror M_2 and was similarly reflected such that it was incident on the beam splitter once again and directed onto the sample surface. Both light beams emerging from the beam splitter were passed through a focal lens (M-LH-0.5A, Newport) before being incident on the thin film surface in order to induce the nanoparticle.

As shown in Fig. 1, mirror M_1 was positioned at different distances from the beam splitter so they have traveled the different paths. The resulting optical path difference (OPD) between the two rays incident on the sample surface is given by

$$OPD = 2n_{air}L \tag{1}$$

where n_{air} is the refractive index of air, and L is the physical path length difference between the transmitted and reflected paths in the interferometer (i.e., $L = A - B$). In the present study, the path length difference was achieved by adjusting the transmitted and reflected paths. The path length difference was assigned different values of 0.0532, 0.1, 0.15, and 0.2 mm, respectively, for investigation purposes.

The intensity of the interference light incident on the sample surface is given by

$$I = I_1 + I_2 + 2\sqrt{I_1 I_2} \cos\Phi \tag{2}$$

where I_1 and I_2 are the intensities of beam 1 and beam 2, respectively, and Φ is the phase difference between them (i.e., $\Phi = (\Phi_1 - \Phi_2)$). Rearranging Eqs. (1) and (2), the phase difference can be obtained as

$$\phi = \frac{OPD}{\lambda} \cdot 2\pi = \frac{2n_{air}L}{\lambda} \cdot 2\pi = N \cdot 2\pi \tag{3}$$

Fig. 1 Michelson interferometer apparatus used in present study

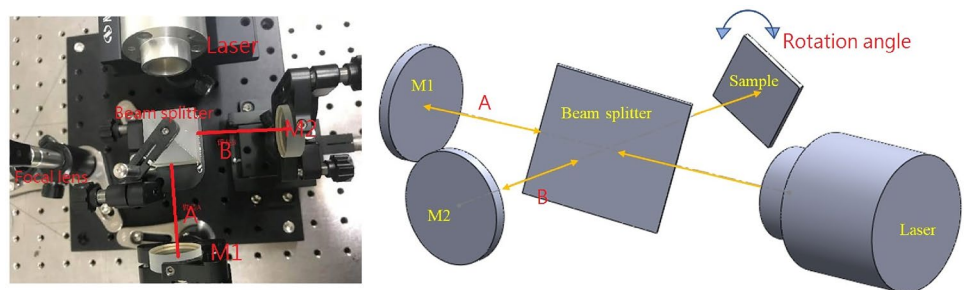


Table 1 Relationship between path length difference (L) and calculated interference fringe order (N)

L	0.0532 mm	0.1 mm	0.15 mm	0.2 mm
N	1000	1879.7	2819.5	3759.4

where N is the interference fringe order. If the path lengths are identical, the two beams interfere constructively with one another, and the maximum interference intensity is obtained. However, if the path lengths deviate by even half wavelength, the two beams are out of phase and interfere destructively.

The experiments commenced by investigating the effects of the laser pulse power, exposure time, and path length difference on the nanoparticle size distribution of the Ag films patterned using the optical setup shown in the left-hand schematic in Fig. 1. A further series of experiments was then performed using the setup shown in the right-hand schematic in Fig. 1, in which the thin-film surface was patterned using a two-step exposure process involving a rotational shift of sample in the range of 30 to 90°. For example, the film was exposed for 5 s to the sample surface and was then irradiated for a further 25 s with the sample rotated through an angle of 30°.

For both sets of experiments, the surface morphologies of the thin films and silver nanoparticles were observed by an optical microscope (OM, HRM-300) and field-emission scanning electron microscope (FE-SEM, JSM-7600F, Japan), respectively. The particle size and distribution

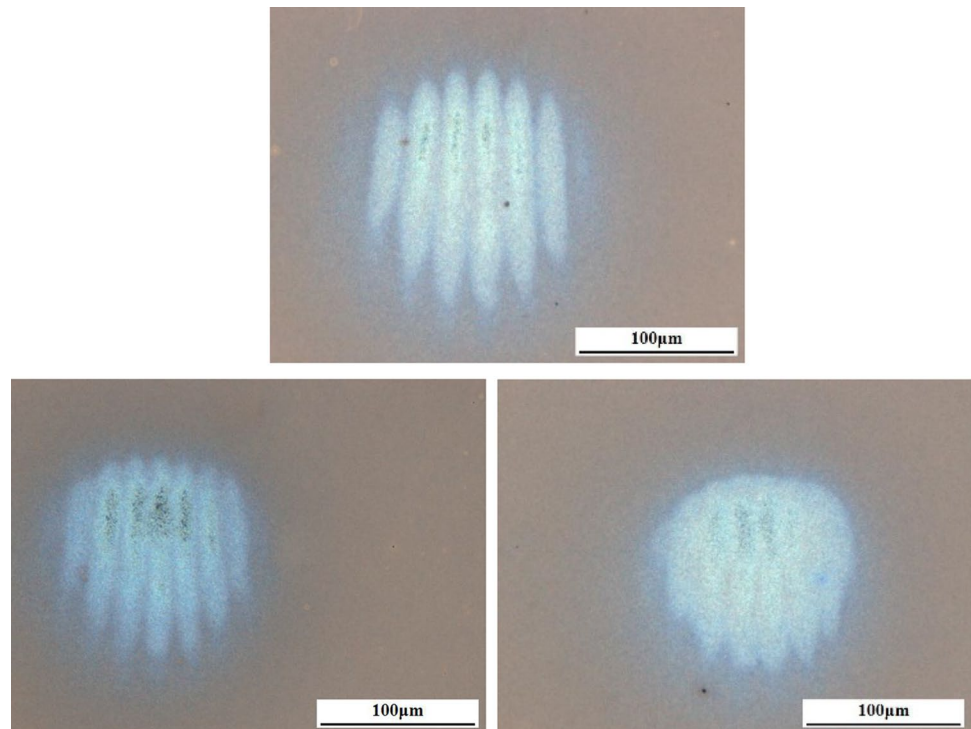
was analyzed using ImageJ software (National Institutes of Health, USA) [26]. In addition, the optical absorbance properties of the interfered films were measured over the wavelength range of 300–1000 nm using a UV–Vis–IR spectrophotometer (Lambda 35, PerkinElmer).

3 Result and discussions

Table 1 shows the relationship between the path length difference (L) in the interferometer system and the calculated interference fringe order. It is clear that the period of the grating structure can be effectively controlled by adjusting the distance between the interfering beams. For example, given a path length difference of 0.0532 mm, the calculated interference fringe number is 1000. However, for a greater path length difference of 0.2 mm, the fringe order increases to 3759. In other words, the interference fringe order increases with an increasing path length difference, as shown in Fig. 2. The measured interference pitch had a value of approximately 20 μm for a path length difference of 0.0532 mm and reduced to 13 μm given the maximum path length difference of 0.2 mm (see Fig. 3). In other words, the interferometer system was capable of patterning micro-gratings with a feature size of 13–20 μm on the Ag surface.

Figure 4 shows the SEM morphologies of the Ag thin films patterned using laser pulse powers in the range of 0.6 to 1.0 W and exposure times ranging from 4 to 600 s. Note that the path length difference is equal to 0.0532 mm in

Fig. 2 OM images of interference Ag thin films processed at 0.6 W and 4 s with path length differences of (a) 0.0532 mm, (b) 0.1 mm, and (c) 0.15 mm



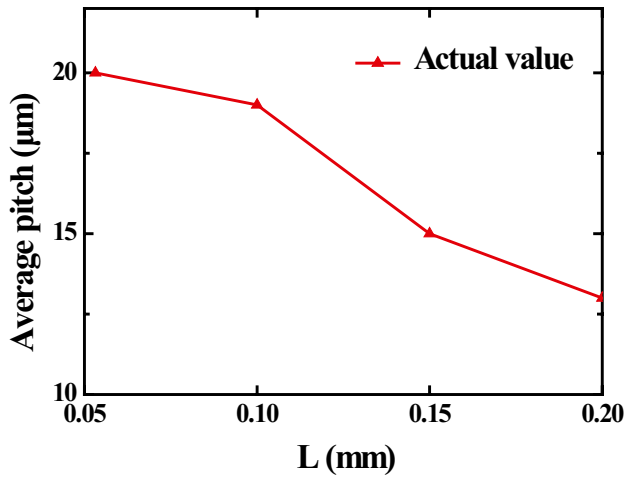


Fig. 3 Relationship between path length difference and measured interference fringe order pitch

every case. It is seen that the nanoparticle size decreases slightly with an increasing power and exposure time. Moreover, distinct island structures are observed at lower values of the laser power and exposure time, as reported previously in [27] for the pulsed-laser interference patterning of thin Au films. In general, the results confirm that the Ag film transforms into nanoparticles with different dimensions under the effects of the energy input accumulated over repeated laser pulses. Horwood et al. [16] reported that pulsed-laser exposure induced a dewetting of Au thin films on Ta₂O₅ substrates only under certain laser fluences and exposure times. In [16], dewetting was not observed at laser fluences less than 200 mJ·cm⁻². Therefore, the Ag film was fully transformed into nanoparticles given the use of a high laser power (1 W) and shorter exposure time (300 s).

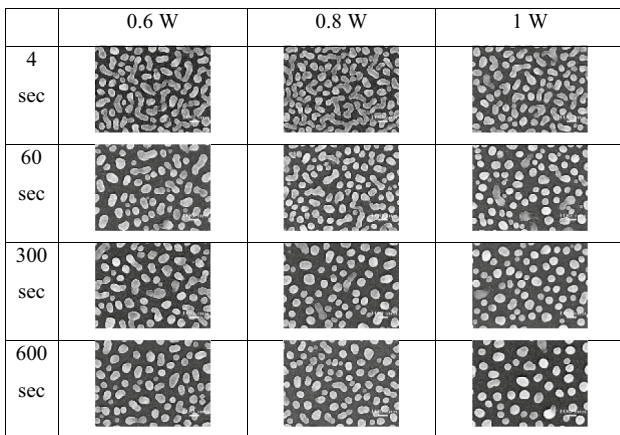


Fig. 4 SEM images of interference Ag thin films processed with different laser powers and exposure times for constant path length difference of $L=0.0532$ mm. (Note that all scale bars are equal to 100 nm.)

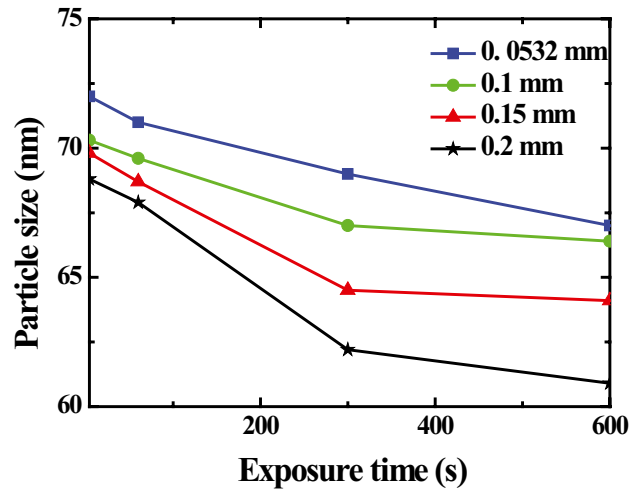


Fig. 5 Variation of particle size with exposure time for constant laser power of 1 W and different path lengths

Figure 5 shows variation of the particle size with the laser pulse exposure time for a constant laser power of 1 W and various path lengths. The results confirm that the particle size decreases with an increasing exposure time. Moreover, for a constant exposure time, the particle size decreases with an increasing path length difference. For example, given the maximum exposure time of 600 s, the particle size decreases from 67 to 61 nm as the path difference length increases from 0.0532 to 0.2 mm. According to this study, Au film was annealed by CO₂ laser, and the formation of nanostructures was observed as confirmed by the optical absorption spectra [28]. In general, the results confirm that, for a constant power, different spot distances result in different surface topographies [29]. In particular, area roughness decreased with an increasing spot distance. This is consistent with the optical absorption spectra for the surface topography.

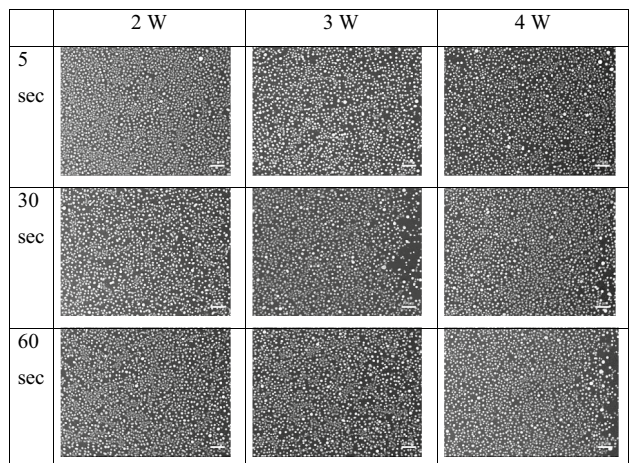


Fig. 6 SEM images of interference Ag thin films processed with different laser powers and exposure times for constant path length difference of $L=0.0532$ mm. (Note that all scale bars are equal to 10 µm.)

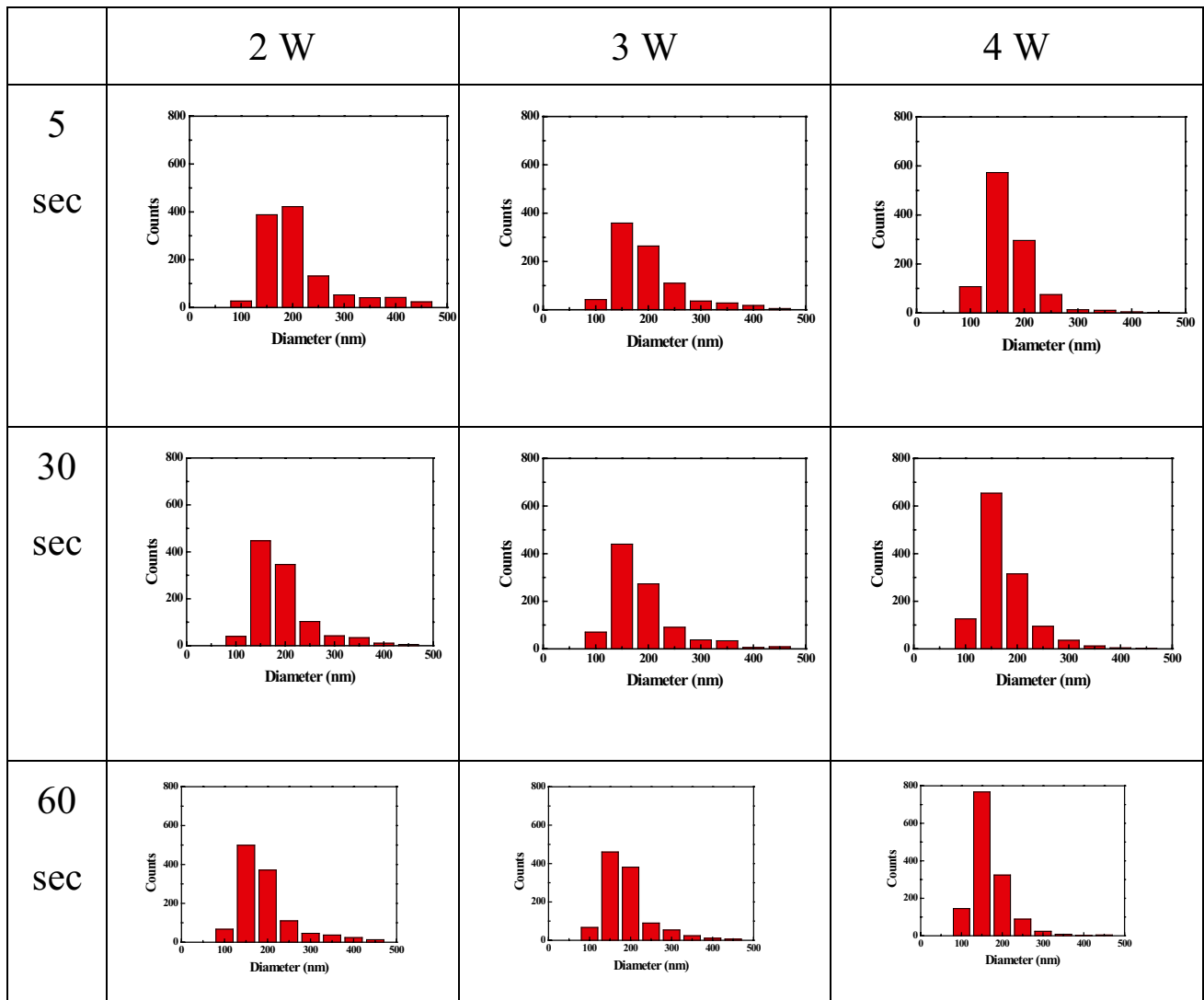
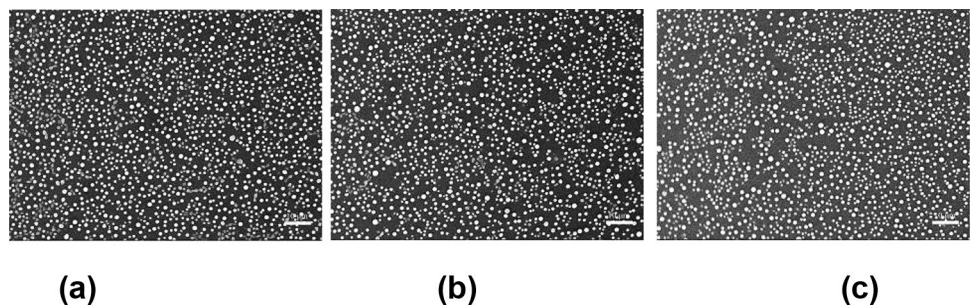


Fig. 7 Particle size distributions for different exposure times and laser powers

Figure 6 presents SEM images of the Ag films patterned using higher pulse laser powers of 2~4 W, shorter exposure times of 5~60 s, and a constant path length difference of $L=0.0532$ mm. Comparing the results presented in Fig. 6 with those in Fig. 4 for a lower pulse laser power and longer exposure time, it is seen that nanoparticles are still produced

in the Ag thin film given a power of 2 W (or more) provided that the exposure time is limited to less than 60 s. Figure 7 shows the particle size distribution of the Ag surfaces shown in Fig. 6. The results confirm that the particle size decreases with an increasing laser power and exposure time. The results are thus consistent with those reported

Fig. 8 SEM images of interference Ag thin films processed using laser power of 3 W and exposure times of 5 s/25 s at rotation angles of (a) 30°, (b) 60°, and (c) 90°. (Note that all scale bars are equal to 10 μm.)



in [30] for the formation of nanoparticles in pure Cu films using a pulsed-laser dewetting process. From inspection, the particle size in the present Ag films reduces from 190 nm under exposure conditions of 2 W-5 s to 150 nm at 4 W-60 s. According to some references [31, 32], it is apparent that the particle size and shape of the dewetted films were found to be dependent on the magnitude of the energy accumulated in the film. Therefore, the NP size reduces due to its accumulated energy.

Figure 8 presents SEM images of the Ag thin films processed using the two-step exposure method with a power of 3 W, an exposure time of 5 s/25 s, and rotation angles of 30, 60, and 90°, respectively. With an increasing total exposure time, the particle size reduced. For both 5 s/25 s and 5 s/55 s samples, the particle size decreased from 173 to 166 nm at a power of 2 W and a rotation angle of 30°. In addition, fixed the total exposure time, the smaller particle would be induced by the shorter first-step exposure time. For both 5 s/25 s and 10 s/20 s samples, the particle size increased from 173 to 183 nm at a power of 2 W and rotation angle of 30° (Fig. 9). Moreover, the particle size increased with an increasing rotation angle. Therefore, it is apparent that the particles are highly dependent on the exposure time and rotation angle. Figure 9 presents the ImageJ analysis results for the particle size distributions of the Ag films processed using laser pulse powers of 2, 3 and 4 W, respectively, and various rotation angles and exposure times. The results confirm that, for a constant pulse power, the particle size increases with an increasing rotation angle. Furthermore, for a constant rotation angle and exposure time, the particle size reduces with an increasing laser power. For example, given a rotation angle of 90° and an exposure time of 5 s/25 s, the particle size reduces from 205 to 122 nm as the laser power increases from 2 to 4 W, respectively. Finally, for a given laser power and rotation angle, the particle size decreases with an increasing total exposure time. Overall, the results show that the minimal particle size is approximately 110 nm at a rotation angle of 30°, an exposure time (second step) of 55 s, and a laser power of 4 W. It is noted that the present findings are consistent with those of Peter et al. [33], who showed that two-dimensional structures can be obtained in stainless steel using a line interference pattern by adding a second process step in which the surface is rotated by 90° [33].

Figure 10 presents the absorption spectra of the Ag films processed using laser pulse powers in the range of 2~4 W and rotation angles of 0, 30, 60, and 90°, respectively. It can be seen that the absorption peak wavelength undergoes a red shift as the rotation angle increases and a blue shift as the laser power increases. The absorption peak wavelength varies between 434 and 465 nm depending on the size of the nanoparticles. It is noted that this value is consistent with that of 430 nm reported by Oh and Lee [21] for dewetted

Ag films with an average particle size of 37 nm. Overall, the results indicate that the resonance band of the patterned gratings undergoes a red shift as the nanoparticle size increases and a blue shift as the particle size decreases.

Observing Fig. 10, it is evident that the half-height widths of the absorption peaks for the films patterned with different rotation angles are wider than that of the films patterned without rotation. In other words, it is inferred that the films

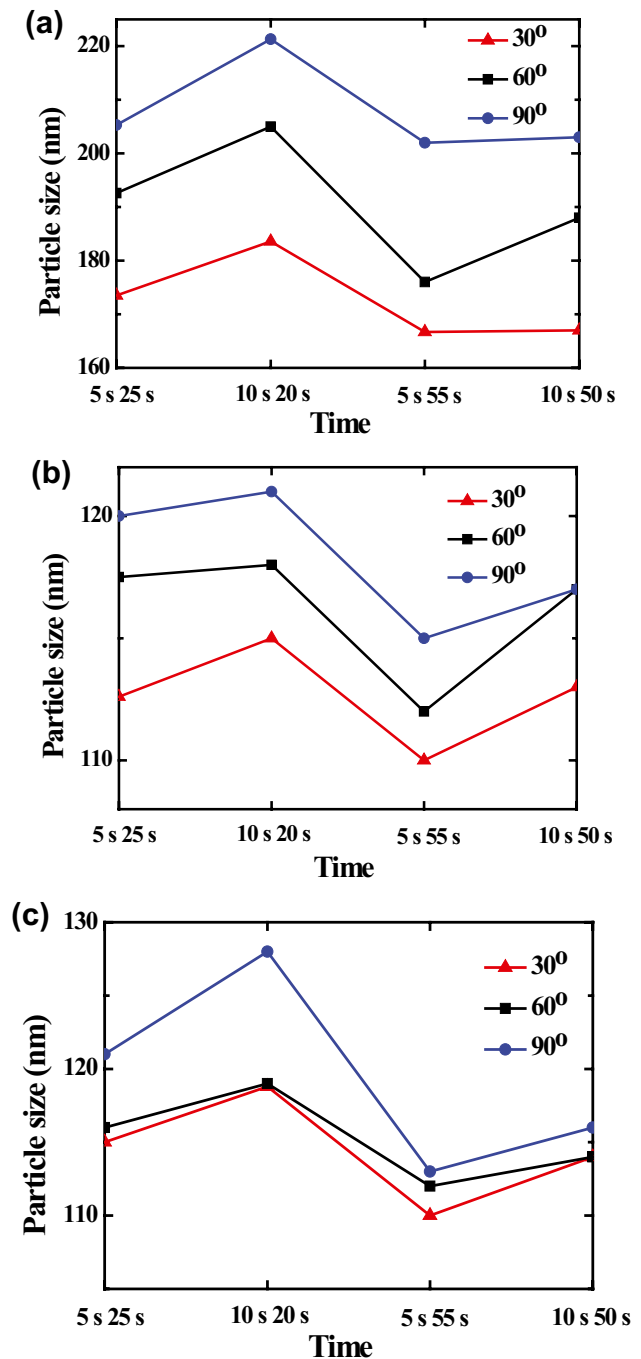


Fig. 9 Particle size distributions for different exposure times and laser powers of (a) 2 W, (b) 3 W, and (c) 4 W

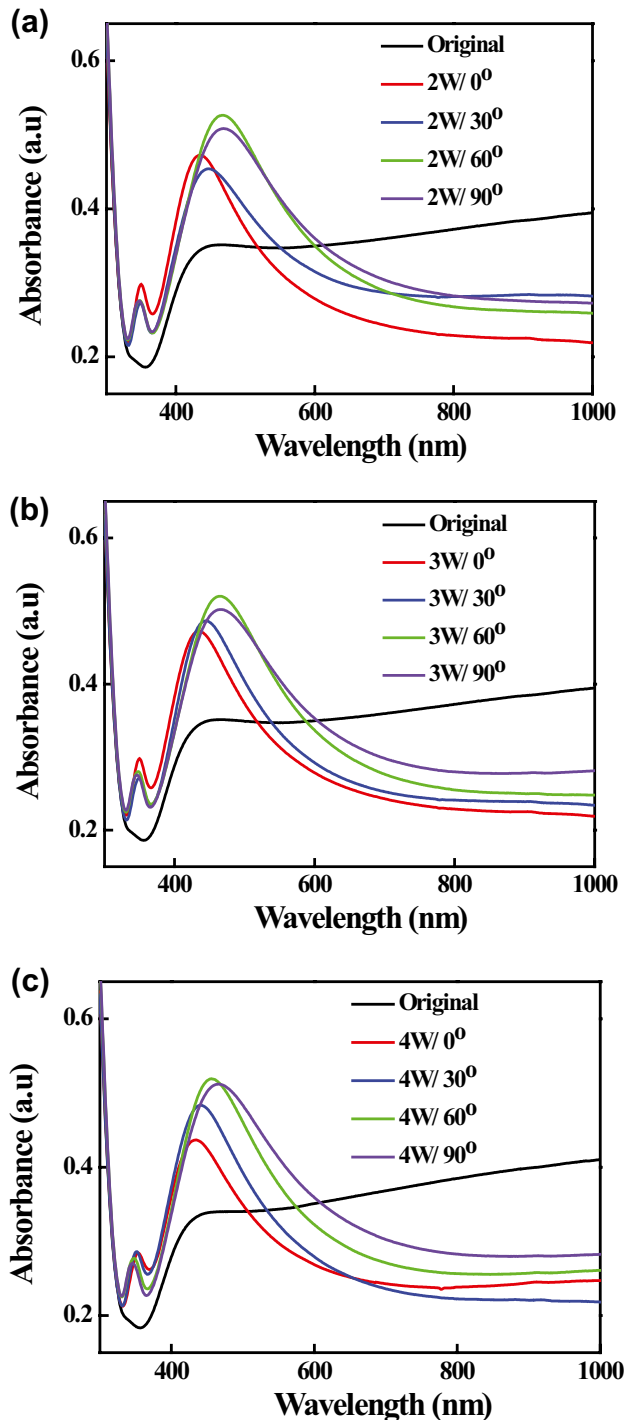


Fig. 10 Absorption spectra of interference films processed using exposure time of 25 s and laser powers of (a) 2 W, (b) 3 W, and (c) 4 W

patterned with two-step rotation exposure have a wider particle size distribution. Moreover, the half-height width value increases with an increasing rotation angle, suggesting that a larger rotation angle broadens the particle size distribution.

It is consistent with the result in Fig. 8, and the particle sizes are uniform at lower rotation angle of 30° .

4 Conclusions

Pure Ag thin films with a thickness of 10 nm were deposited on glass substrates and patterned with periodic grating structures using a Michelson interferometer dewetting process. The effects of the laser pulse power, exposure time, and path length difference on the size distribution of the resulting Ag nanoparticles were systematically explored. The nanoparticle size was found to decrease from 67 to 61 nm as the path length difference increased from 0.0532 to 0.2 mm. Moreover, the particle size also decreased with an increasing exposure time and laser power. In particular, the particle size reduced from 190 nm for a laser power and exposure time of 2 W and 5 s, respectively, to 150 nm for a laser power and exposure time of 4 W and 60 s.

A second series of experiments was performed in which the Ag films were exposed in a two-step process involving a rotation angle in the range of $30^\circ \sim 90^\circ$ and a modified exposure time. For a constant laser power, the particle size increased with an increasing rotation angle. By contrast, for a constant rotation angle, the particle size decreased with an increasing laser power and total exposure time. The minimum particle size was found to be around 110 nm for a rotation angle of 30° , a laser power of 4 W, and a second-step exposure time of 55 s. The absorption peak wavelength of the Ag interfered films underwent a red shift as the rotation angle increased, but underwent a blue shift as the laser power increased (the particle size decreased). Finally, the half-height widths of the absorption peaks in the Ag films processed using different rotation angles were found to be wider than those of the absorption peaks in the films processed without rotation, indicating that the rotation process resulted in a wider particle size distribution. Overall, the results presented in this study show that the structural and optical properties of Ag thin films patterned using a laser interference dewetting process are highly dependent on the interference parameters.

Author contribution Hsuan-Kai Lin: writing, review, and funding acquisition. Ying-Chi Chen: investigation, formal analysis, data collection, visualization, and writing. Jia-Ren Lee: conceptualization, formal analysis, and review. Wei-Hua Lu: original draft, resources and visualization. Yuan-Jen Chang: review, methodology and editing.

Funding The authors received financial support provided by the Ministry of Science and Technology of Taiwan, ROC, under Project No. MOST 109-2637-E-020-001.

Data availability All data generated or analyzed during this study are included in the present article.

Declarations

Ethics approval Not applicable.

Consent to participate Not applicable.

Consent for publication Not applicable.

Competing interests The authors declare no competing interests.

References

- Chong TC, Hong MH, Shi LP (2010) Laser precision engineering: from microfabrication to nanoprocessing. *Laser Photonics Rev* 4(1):123–143
- Kaganovskii Y, Vladimirovsky H, Rosenbluh M (2006) Periodic lines and holes produced in thin Au films by pulsed laser irradiation. *J Appl Phys* 100(4):044317
- Wang X, Chen F, Liu H, Liang W, Yang Q, Si J, Hou X (2009) Fabrication of micro-gratings on Au–Cr thin film by femtosecond laser interference with different pulse durations. *Appl Surf Sci* 255(20):8483–8487
- Milles S, Soldera M, Kuntze T, Lasagni AF (2020) Characterization of self-cleaning properties on superhydrophobic aluminum surfaces fabricated by direct laser writing and direct laser interference patterning. *Appl Surf Sci* 525:146518
- Lechthaler B, Fox T, Slawik S, Mücklich F (2020) Direct laser interference patterning combined with mask imaging. *Opt Laser Technol* 123:105918
- Kim D, Ji R, Fan H, Bertram F, Scholz R, Dadgar A, Nielsch K, Krost A, Christen J, Gösele U, Zacharias M (2007) Laser-interference lithography tailored for highly symmetrically arranged ZnO nanowire arrays. *Small* 3(1):76–80
- Rosenfeld A, Rohloff M, Höhm S, Krüger J, Bonse J (2012) Formation of laser-induced periodic surface structures on fused silica upon multiple parallel polarized double-femtosecond-laser-pulse irradiation sequences. *Appl Surf Sci* 258(23):9233–9236
- Ihleman J (2005) Ultraviolet laser ablation patterning of oxide films for optical applications. *Opt Eng* 44(5):051108
- Meyer HM, Sabau AS, Daniel C (2019) Surface chemistry and composition-induced variation of laser interference-based surface treatment of Al alloys. *Appl Surf Sci* 489:893–904
- Ströbel J, Voisiat B, Du K, Lasagni AF (2019) How to get deeper structures with the same energy: fabrication of periodic structures in stainless steel using direct laser interference patterning with burst mode ps-pulses. *Mater Lett* 246:121–124
- Peter A, Lutey AHA, Faas S, Romoli L, Onuseit V, Graf T (2020) Direct laser interference patterning of stainless steel by ultrashort pulses for antibacterial surfaces. *Opt Laser Technol* 123
- Liu W, Yu Z, Lu D, Zhang N (2021) Multi-wavelength annular optical pulses generated by double interferent femtosecond Bessel laser beams in silica glass. *Opt Lasers Eng* 136
- Sabau AS, Meyer HM, Leonard DN (2020) Laser-interference pulse number dependence of surface chemistry and sub-surface microstructure of AA2024-T3 alloy. *Opt Laser Technol* 131
- Lechthaler B, Fox T, Slawik S, Mücklich F (2020) Direct laser interference patterning combined with mask imaging. *Opt Laser Technol* 123
- Lin YH, Wang JJ, Wang YT, Lin HK, Lin YJ (2020) Antifungal properties of pure silver films with nanoparticles induced by pulsed-laser dewetting process. *Appl Sci* 10(7)
- Horwood CA, Owusu-Ansah E, Shi YJ, Birss (2021) Pulsed laser induced dewetting of Au thin films on Ta₂O₅ substrates. *Chem Phys* 541
- Kim H, Shin H, Ha J, Lee M, Lim KS (2007) Optical patterning of silver nanoparticle Langmuir-Blodgett films. *J Appl Phys* 102(8):083505
- Riedel S, Schmotz M, Leiderer P, Boneberg J (2010) Nanostructuring of thin films by ns pulsed laser interference. *Appl Phys A* 101(2):309–312
- Aktag A, Michalski S, Yue L, Kirby RD, Liou SH (2006) Formation of an anisotropy lattice in Co/Pt multilayers by direct laser interference patterning. *J Appl Phys* 99(9):093901
- Mason DR, Gramotnev DK, Gramotnev G (2008) Thermal tweezers for manipulation of adatoms and nanoparticles on surfaces heated by interfering laser pulses. *J Appl Phys* 104(6):064320
- Oh Y, Lee M (2017) Single-pulse transformation of Ag thin film into nanoparticles via laser-induced dewetting. *Appl Surf Sci* 399:555–564
- Shiau BW, Lin CH, Liao YY, Lee YR, Liu SH, Ding WC, Lee JR (2018) The characteristics and mechanisms of Au nanoparticles processed by functional centrifugal procedures. *J Phys Chem Solids* 116:161–167
- Oh H, Lee J, Lee M (2018) Transformation of silver nanowires into nanoparticles by Rayleigh instability: Comparison between laser irradiation and heat treatment. *Appl Surf Sci* 427:65–73
- Arya M, Dewasi A, Mitra A (2018) Spectroscopic ellipsometer study of laser ablation wavelength dependent growth kinetics of Ag nanoislands: an insight to potential plasmonic applications. *Appl Surf Sci* 447:87–99
- Ruffino F, Grimaldi MG (2019) Nanostructuring of thin metal films by pulsed laser irradiations: a review. *Nanomaterials* (Basel) 9(8)
- Gorji NE, O'Connor R, Brabazon D (2021) XPS, SEM, AFM, and nano-indentation characterization for powder recycling within additive manufacturing process, IOP Conference Series: Mater Sci Eng 1182(1):012025
- Peláez RJ, Baraldi G, Afonso CN, Riedel S, Boneberg J, Leiderer P (2012) Selective gold nanoparticles formation by pulsed laser interference. *Appl Surf Sci* 258(23):9223–9227
- Maurya SK, Uto Y, Kashihara K, Yonekura N, Nakajima T (2018) Rapid formation of nanostructures in Au films using a CO₂ laser. *Appl Surf Sci* 427:961–965
- Baumann R, Milles S, Leupolt B, Kleber S, Dahms J, Lasagni AF (2021) Tailored wetting of copper using precise nanosecond direct laser interference patterning. *Opt Lasers Eng* 137
- Lin HK, Wang YT, Chuang WS, Chou HS, Huang JC (2020) Surface resonance properties of pure Cu and Cu₈₀Zr₂₀ metallic glass films with nanoparticles induced by pulsed-laser dewetting process. *Appl Surf Sci* 507:145185
- Lin HK, Wang JJ, Lu WH, Chuang WS, Chen CY, Chou HS, Huang JC (2021) Microstructure and optical properties of AgCuAl medium entropy films with nanoparticles induced by pulsed-laser dewetting. *Surf Coat Technol* 421:127427
- Lin HK, Huang CW, Lin YH, Chuang WS, Huang JC (2021) Effects of accumulated energy on nanoparticle formation in pulsed-laser dewetting of AgCu thin films. *Nanoscale Res Lett* 16(1):110
- Peter A, Lutey AHA, Faas S, Romoli L, Onuseit V, Graf T (2020) Direct laser interference patterning of stainless steel by ultrashort pulses for antibacterial surfaces. *Opt Laser Technol* 123:105954

Publisher's Note Springer Nature remains neutral with regard to jurisdictional claims in published maps and institutional affiliations.